Nanoscale

Accepted Manuscript

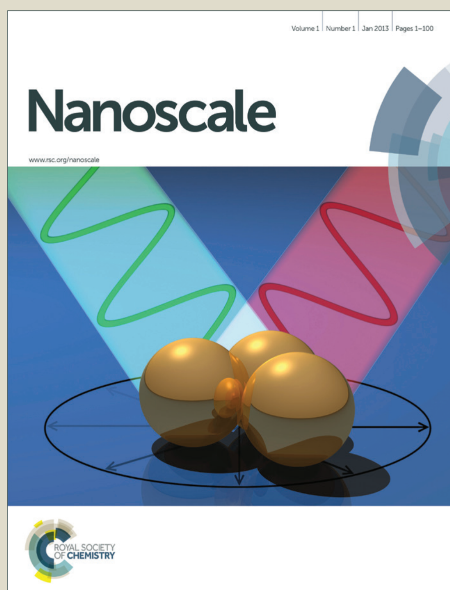

This is an *Accepted Manuscript*, which has been through the Royal Society of Chemistry peer review process and has been accepted for publication.

Accepted Manuscripts are published online shortly after acceptance, before technical editing, formatting and proof reading. Using this free service, authors can make their results available to the community, in citable form, before we publish the edited article. We will replace this *Accepted Manuscript* with the edited and formatted *Advance Article* as soon as it is available.

You can find more information about *Accepted Manuscripts* in the Information for Authors.

Please note that technical editing may introduce minor changes to the text and/or graphics, which may alter content. The journal's standard Terms & Conditions and the Ethical guidelines still apply. In no event shall the Royal Society of Chemistry be held responsible for any errors or omissions in this *Accepted Manuscript* or any consequences arising from the use of any information it contains.

ROYAL SOCIETY OF CHEMISTRY

www.rsc.org/nanoscale

Nanoscale RSCPublishing

ARTICLE

Cite this: DOI: 10.1039/x0xx00000x

Received 00th January 2014,
Accepted 00th January 2014

DOI: 10.1039/x0xx00000x

www.rsc.org/

High-sensitive and Multispectral Responsive Phototransistor Using Tungsten-Doped VO_2 Nanowires

Junpeng Lu,[†a] Hongwei Liu,[†b] Suzi Deng,[a] Minrui Zheng,[a] Yinghui Wang,[a] Jeroen A. van Kan,[a] Sing Hai Tang,[a] Xinhai Zhang,[*c] Chorng Haur Sow[*a] and Subodh G. Mhaisalkar[d]

In this work, we report a novel and feasible strategy for practical application of one-dimensional ultrasensitive phototransistors made of tungsten-doped VO_2 single nanowires. The photoconductive response of the single nanowire device was investigated under different visible light excitations (405 nm, 532 nm, and 660 nm). The phototransistor device exhibited ultrafast photoresponse, high responsivity, broad multispectral response, and rapid saturation characteristic curve. These promising results help to promote the applications of this material in nano-scaled optoelectronic devices such as efficient multispectral phototransistors and optical switches.

Nanoscale Accepted Manuscript

Introduction

Photoconductions in nanowires have attracted lots of attention due to their unique properties that contribute to the high photosensitivity of such nanostructures.[1-6] Firstly, the large surface to volume ratio and the existence of surface trap states in nanowires could greatly prolong the photocarrier life time. In addition, the reduced size of the active working region in nanowire device shortens the carrier transit time. Indeed, the concurrence of the long life time and short transit time of photocarriers will facilitate substantial photoconductive gain.[7, 8] These promising properties result in the applications of the semiconductor nanowires as photodetectros, photovoltaics, optical switches, and optical interconnects.[9-13] Among these applications, phototransistor is an attractive device as it is one of the basic building blocks for nano-optoelectronic circuits. In the last decade, extensive research effort has been devoted to such device due to its significantly lower noise and higher sensitivity than those of other counterparts.[14, 15] However, reported phototransistors faced the challenges of slow response rate[16-18] or excessively high working voltage (> 10 V),[19-21] restraining the performance of the optoelectronic devices. Furthermore, the saturation of the output current is not easy to achieve, which would confine the rectification application of the transistors. [16, 22] Among the metal oxide nanowires, vanadium dioxide (VO_2) nanowires have attracted great attention.[23, 24] Research interests on this nanostructure focus on its metal-insulator transition and related properties.[25-27] However, little attention has been paid to the optoelectronic applications of VO_2 due to its low photoresponse at room temperature, whilst its low n-type electrical conductivity always inhibits its practical application implementation as well. Impurity doping is one of the most commonly employed techniques to modify the electrical properties of a material. Recently, the substitutional doping of both the vanadium and oxygen sublattices have been extensively explored to appreciably reduce the phase transition temperature.[28, 29] Substituting the vanadium with tungsten is particularly attractive and results in a depression in the phase transition in vanadium oxide.[30, 31] Most recently, W-doped VO_2 1D nanostructure was synthesized and its phase transition property was shown to be influenced by the combination of doping and finite size.[32] However, the study of optoelectronic property and corresponding application of such W-doped VO_2 nanostructures are still absent up to date. In this work, we present a comprehensive study on the optoelectronic property of W-doped VO_2 nanowires. The work begins with the solution synthesis of tungsten doped VO_2 nanowires by a facile hydrothermal approach. Upon the substitution of vanadium with tungsten, the electron donor levels become extremely shallow, facilitating supersensitive phototransistive process and yielding an ultrafast photocurrent response along with a broad multispectral response. In addition, saturation of the light intensity gated output current could be easily achieved within the bias of 1.5 V. We analyzed the charge transport under laser irradiation with different wavelength and a series of light

intensity. We found that the device could be controlled readily. These results demonstrate the great potential of tungsten doped VO_2 nanowires in nano-scaled optoelectronic applications.

Experimental Section

The synthesis of tungsten-doped VO_2 nanowires employed a simple and template-free hydrothermal method.[33] Briefly, 0.5 g of V_2O_5 powder was dispersed in 40 mL of deionized water (ρ = 18.2 MΩ cm^{-1}) under vigorous stirring. Subsequently, 0.6 g of $H_2C_2O_4$ (oxalic acid) mixed with 0.03 g of H_2WO_4 (tungstic acid) was slowly added into this dispersion. After stirring for 3 hours to yield a bright orange suspension, the resulting mixture was transferred into a 50 mL Teflon container and then sealed in an autoclave using a high-pressure Parr acid digestion bomb. The autoclave was kept in an oven and the system temperature was ramped to 250 °C and dwelled for 72 hours. After cooling to room temperature, dark blue precipitates were collected. The product was washed with acetone solution and deionized water several times, and then dried in a vacuum condition at 70 °C for overnight.

After the synthesis, a single W-doped VO_2 nanowire was transferred to a silicon substrate coated with a 200 nm thick Si_3N_4 dielectric layer for device fabrication and subsequent electronic characterization. A UV laser lithography system (Heidelberg Instruments µPG101) was used to fabricate the device. The device fabrication was completed by thermal evaporation of 20 nm cobalt and 280 nm gold as the source-drain electrodes.

The single nanowire phototransistor characterization was carried out by irradiating the nanowire with a laser beam bigger than the size of the nanowire in a high vacuum chamber. For the carrier life time determination, a focused laser beam from a diode laser in conjunction with a modified optical microscope was employed. The focused laser beam system was a home-built scanning photocurrent microscopy (SPCM) unit. SPCM is an ideal technique for probing various physical properties from one dimensional nanostructures, such as local band bending, barrier heights, electrical field distribution, and carrier diffusion lengths.[34-40] Our SPCM set-up, involves irradiating a focused laser spot (< 1µm) on a selected position of a planar device while recording the photocurrent as a function of the focused laser spot, i.e., local photo-carrier injection position. The measurements were carried out by utilizing Keithley 6430 sourcemeter under a constant bias. A heating stage (Linkam Scientific Instruments, TMS 94) was employed for the thermal cycling experiments.

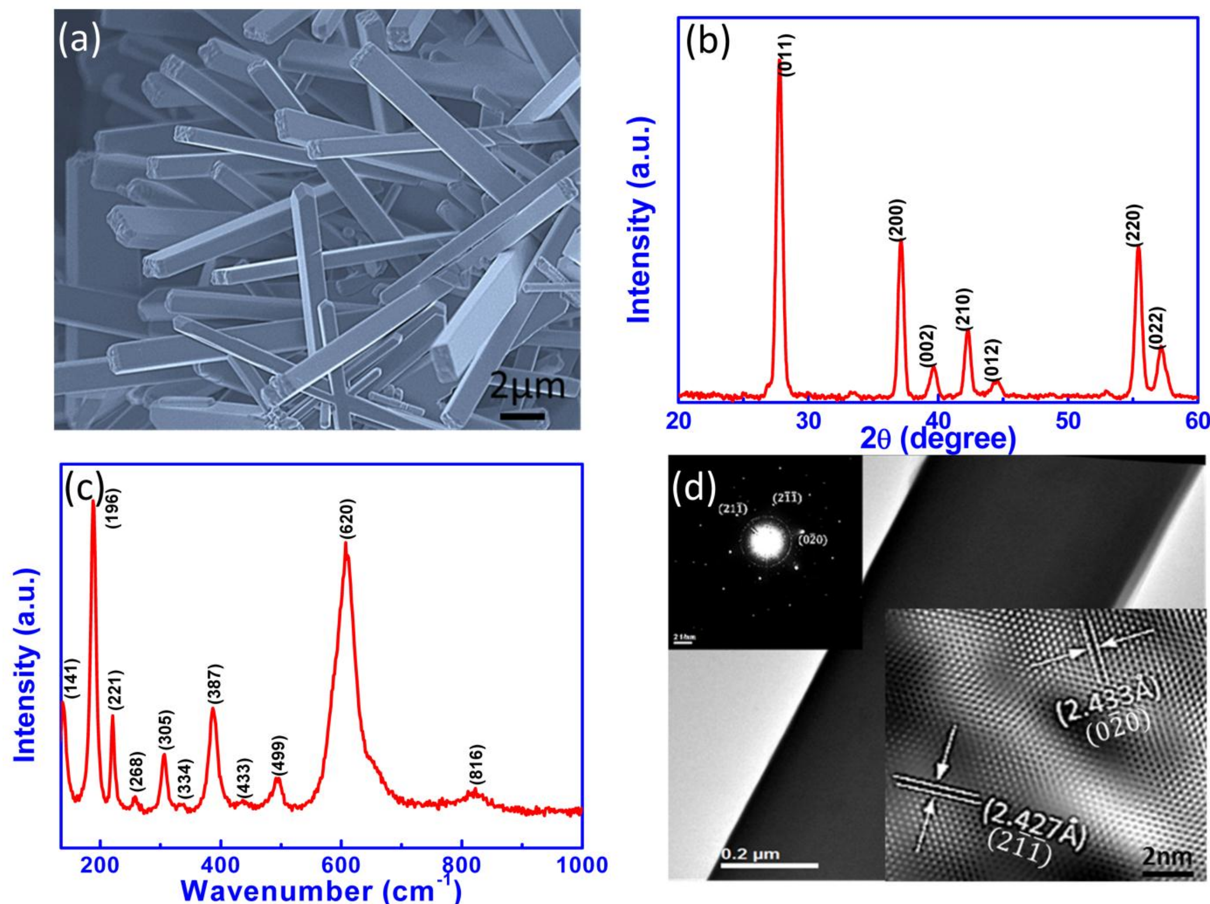

Figure 1. (a) SEM image of the as-synthesized nanowires. (b) XRD spectrum of the nanowires indicates the stable monoclinic polymorph. (c) Raman spectrum of the nanowires. (d) Low-magnification TEM image of a single nanowire. Inserts show the SAED and HRTEM of the nanowire.

Nanoscale Accepted Manuscript

This journal is © The Royal Society of Chemistry 2012

Results and Discussions

The morphology of the as-synthesized products was characterized by scanning electron microscopy (SEM). A typical SEM image of the nanowires is shown in Figure 1a. The nanowires exhibit rectangular cross-sections with smooth and well faceted surfaces. The typical size of the cross-section of the as-synthesized nanowires is in the range of 300-800 nm and the length is in the range of 5-30 μm. The XRD patterns recorded from the nanowires drop-casted on a Si substrate is shown in Figure 1b. The peaks obtained can be indexed to the stable monoclinic VO_2 (M1) polymorph. We do not see any signals for the formation of metastable VO_2(B) polymorph due to the high temperature environment during the synthesis.[32] As compared with undoped VO_2, the interplanar spacing increases after substitutional W incorporation. This is consistent with the larger atomic radius of the dopant W^{6+} ion[33] and the possible existence of M2 phase.[41] Further structural characterization of the nanowires was carried out by micro-Raman spectroscopy. Figure 1c depicts room temperature Raman spectrum of W doped VO_2 nanowires. The space group for M1 and M2 lattices are C_{2h}^{3}, and C_{2h}^{5}, respectively.[42] Therefore, the M1 phase is characterized by 18 Raman-active modes, with $9A_g$ and $9B_g$ modes, by group theory.[43] The M2 phase also has 18 Raman active modes with slightly different distributions, with $10A_g$ and $8B_g$ modes, due to the pronounced differences in local symmetry.[44] The Raman spectrum in Figure 1c is consistent with previously reported Raman studies and group theory predictions,[45-47] despite of the small shifts of the 607 and 189 cm^{-1} A_g modes to 620 and 196 cm^{-1}, respectively. The shift is probably due to the tungsten doping[33] or the existence of the M2 phase resulting from the incorporation of the substitutional W dopant.[41] Transmission electron microscopy (TEM) was employed to investigate the crystalline lattice of the W doped VO_2 nanowires. Figure 1d illustrates the low-magnification TEM image of a single nanowire, the corresponding selected area electron diffraction (SAED) and high-resolution TEM (HRTEM) images. The fringe spacings between adjacent lattice planes are measured to be 2.433 Å and 2.427 Å, corresponding to the $(0\bar{2}0)$ and $(2\bar{1}\bar{1})$ interplanar distance, respectively.

Figure 2a illustrates schematically the architecture of the fabricated single nanowire phototransistor device and the corresponding SEM image of the device with two finger electrodes shown in the inset of Figure 2b. The separation between two electrodes is 15 μm. The energy-dispersive spectroscopy (EDX) was carried out on randomly selected spots along the nanowire, and the representative spectrum is shown in Figure 2b. The tungsten peak is clearly demonstrated, which indicates the W atoms have been doped into VO_2 successfully. We denote the W-doped VO_2 nanowire as $W_xV_{1-x}O_2$, where x denotes the atomic ratio of W as the fraction of the substituted vanadium sublattice. As revealed by the EDX spectrum, the utilized VO_2 nanowire is doped with about 0.42 at% W. Since metal-insulator transition is a notable feature of VO_2,[48, 49] we measured the temperature dependent electrical resistance from the single $W_xV_{1-x}O_2$ nanowire device. As shown in Figure 2c, with increasing temperature, the two-terminal resistance steadily decreases, presenting classical activated semiconductor transport property, and switches over to metallic behavior with temperatures above 50 °C. Upon cooling, the nanowire displays a reverse jump to the insulating phase at a lower temperature of 27 °C, thus a pronounced hysteresis is exhibited. The phase transition temperature is significantly lower than the pure VO_2 nanowires (67 °C), which is due to the increased free carrier density with W doping. This result is consistent with the behavior of $W_xV_{1-x}O_2$ nanobelts reported by Banerjee and co-workers.[32]

Figure 2d shows the typical *I-V* curves of the nanowire device in dark condition and under a 532 nm broad laser beam illumination with the light intensity of 25 mW cm^{-2} and 50 mW cm^{-2}, respectively. The voltage was swept from 0 to 4 V and all the measurements were carried out at room temperature. Due to the higher work function of the metal electrodes, the metal-semiconductor junction resulted in the formation of a Schottky barrier between the nanowire and the Au electrodes.[50] The *I-V* behavior under illumination of 532 nm laser drastically differs from the dark I-V behavior. The *I-V* characteristics under illumination present an obvious non-linear behavior. The output current increases sharply from 0 V and subsequently reaches near saturation at 1.5 V for 25 mW cm^{-2} illumination (2 V for 50 mW cm^{-2} case). A change in magnitude of about 50 μA is observed in this case. The rapid increase and saturation of the photocurrent suggests the potential of $W_xV_{1-x}O_2$ nanowire as an ultrasensitive phototransistor. The dark I-V indicates that the nanowire was highly resistive, while under laser light irradiation (laser wavelength = 532 nm, photon energy = 2.33 eV), the conductance of the nanowire increases significantly. We preliminarily ascribe the dramatic increase to the photogenerated free carriers rather than the light induced phase transition since the laser intensity was carefully controlled well below the phase transition threshold of VO_2, which is about 20 kW cm^{-2} at room temperature.[51] Even though the threshold of laser induced phase transition for $W_xV_{1-x}O_2$ nanowire would be lower than that of VO_2, the power intensity of several tens of mW cm^{-2} is much lower than the expected phase transition threshold of $W_xV_{1-x}O_2$ nanowire. To further support this claim, finite element method (FEM) was employed to simulate the temperature increase caused by the laser irradiation. The result indicates that the local temperature increased from room temperature (298 K) to 304 K at light intensity of 100 mW cm^{-2}, as shown in Figure 2e. This value is much lower than the phase transition temperature.

The output characteristics under the illumination of a series of intensities of 532 nm laser light are shown in Figure 3a. With the increase of incident light power intensity, the output current rises gradually. Evidently, the output current is controlled by the light power intensity, and the output curves display good transistor behavior, consisting of a rapidly increasing linear regime and a fully saturated regime, which is similar to the output characteristics of a traditional field effect transistor controlled by gate voltage, except here the light intensity plays

Nanoscale Accepted Manuscript

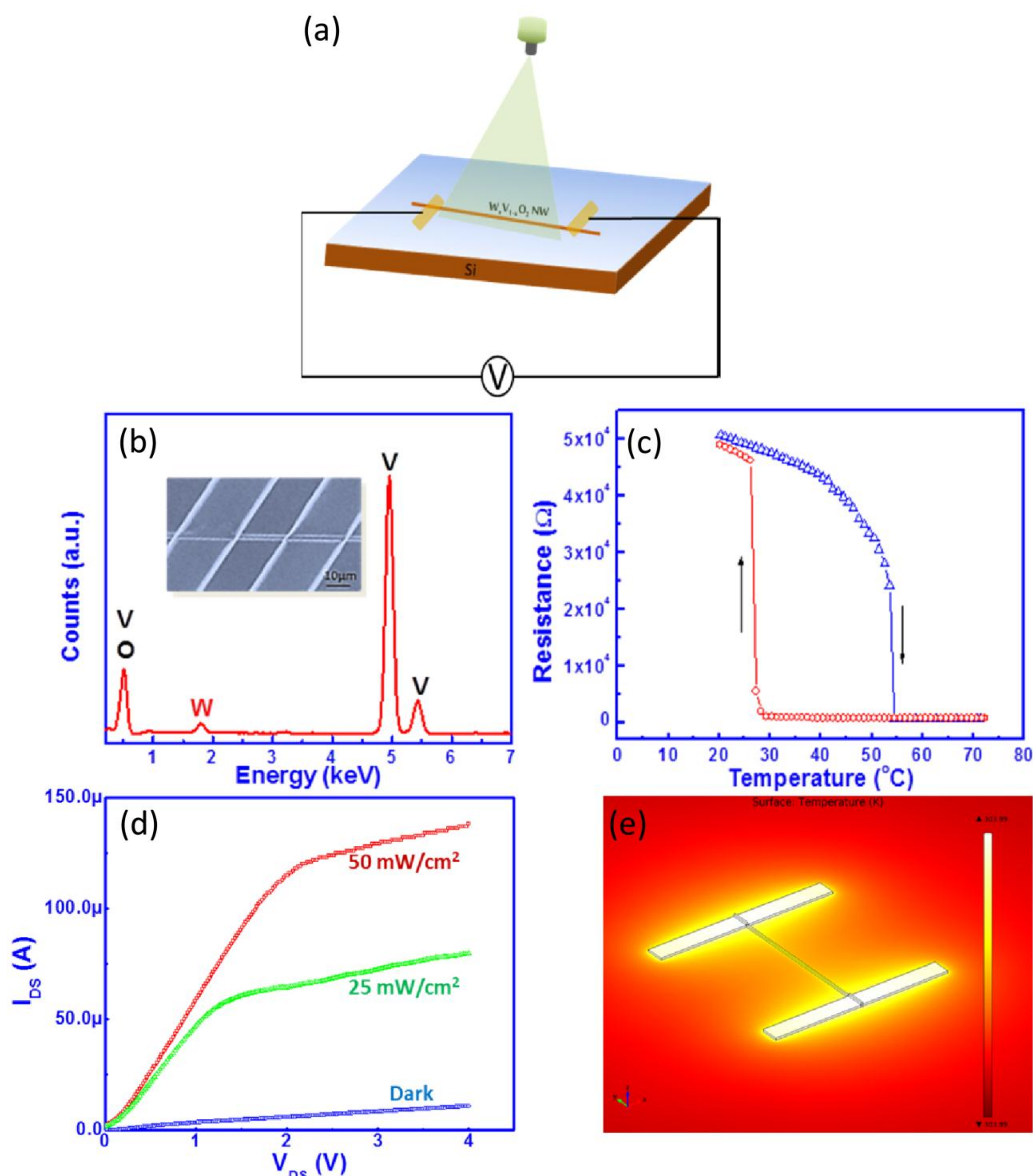

Figure 2. (a) Schematic of a single nanowire device and the broad beam laser setup. (b) EDX spectrum of the single nanowire indicates the tungsten doping. Inserts shows the SEM image of the nanowire device. (c) Metal-insulator transition property demonstration of the $W_xV_{1-x}O_2$ nanowire. (d) I-V curves of the device in dark and under 532 nm laser illumination at intensities of 25 mW cm^{-2} and 50 mW cm^{-2}. (e) Simulation result of the temperature distribution on the nanowire device.

the role of voltage gating. The results suggest that the incident light could be employed to replace the gate voltage, V_{GS}, as an and signal magnification in a single nanowire device for future low-cost, nanoscale photoelectric integration. As described above, the $W_xV_{1-x}O_2$ nanowire phototransistors are expected to show the photoresponse to multispectral light. Figure 3b and 3c show the output characteristics of the nanowire device under different intensities of 405 nm and 660 nm light irradiation, respectively. The similar phototransistor behavior is observed as that under 532 nm light illumination. The output current can also be well controlled by incident light intensity and saturation additional terminal to control the output current of the transistor, indicating an effective approach to achieve current modification is achieved at higher voltages, indicating the wide application potential, easy realizability and flexible maneuverability of the $W_xV_{1-x}O_2$ nanowire phototransistors. Figure 3d shows the variation of photocurrent ($I = I_{photo} - I_{dark}$) measured at the bias of 4 V with light intensity. The photocurrent *versus* illumination light intensity can be described by a power law dependence in the form of $I = AP^{\alpha}$,[52, 53] where I is the photocurrent, A is a proportionality constant, P is the power intensity and the exponent α is an empirical value (usually

Nanoscale Accepted Manuscript

 This journal is © The Royal Society of Chemistry 2012

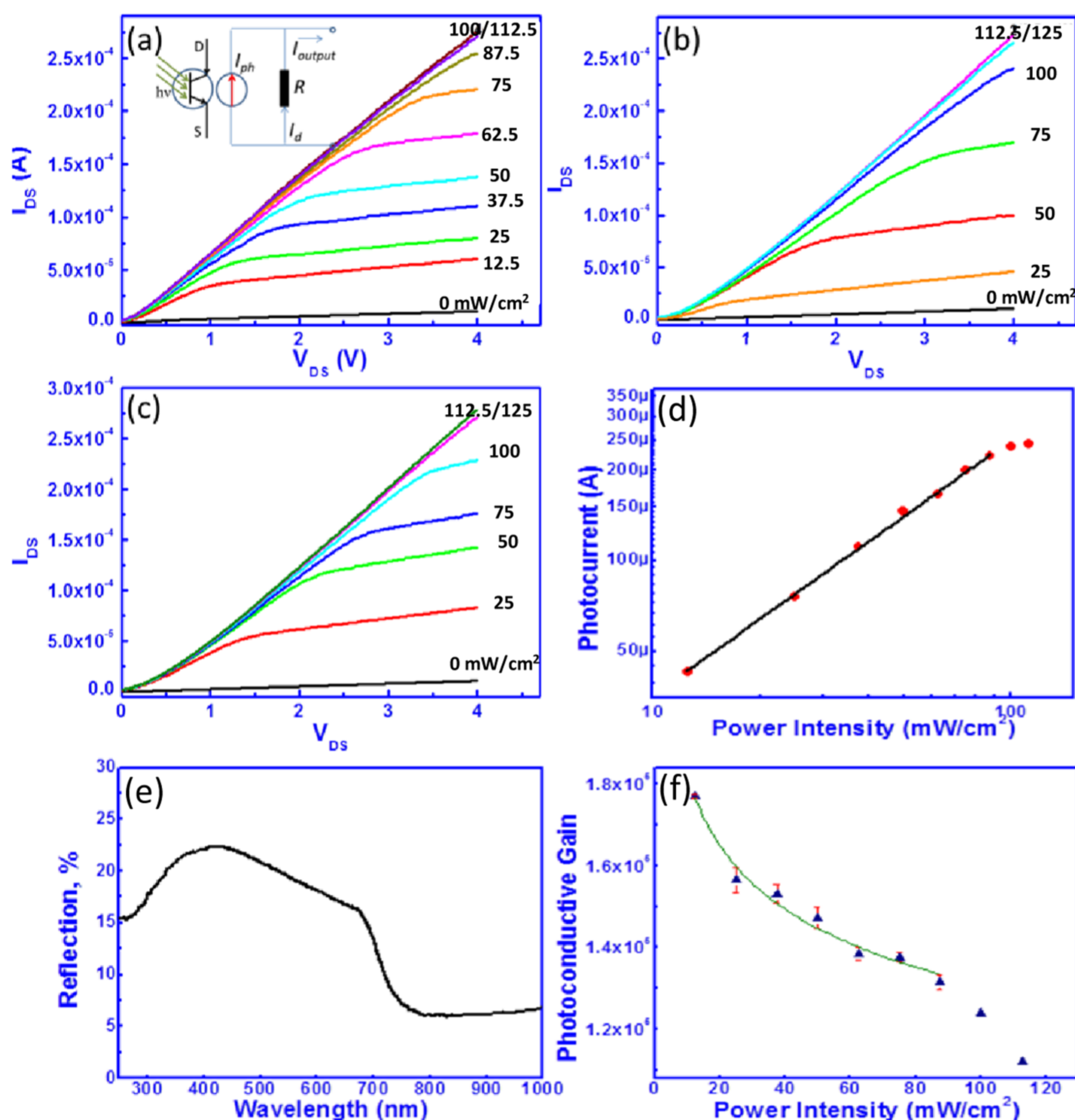

Figure 3. Output characteristics curves of the device under (a) 532 nm, (b) 405 nm, and (c) 660 nm light illumination at different intensity. (d) Photocurrent versus intensity plot at bias of 4 V. (e) Reflection spectrum of as-synthesized nanowires. (f) Photoconductive gain *versus* intensity plot at bias of 4 V.

smaller than unity), determining the photocurrent response to light intensity.[8, 54] As displayed in Figure 3d, the photocurrent *versus* light intensity variation at a bias of 4 V is well fitted with the power law as $I \sim P^{0.82}$ when the light intensity is lower than 100 mW cm^{-2}. The high α value indicates the strong dependence of the photocurrent on light intensity. When there is a uniform distribution of trap states, the photocurrent dependence on the incident light intensity would be linear, consistent with that the photogeneration efficiency of charge carrier is proportional to the absorbed photon flux.[7, 55] The non-integer power dependence of the $W_xV_{1-x}O_2$ nanowire device could be atttibuted to a complex process of carrier generation, recombination and trapping along the nanowire.[10] However, further increase the incident power intensity leads to the photocurrent satuaration at higher light intensity (beyond 100 mW cm^{-2}). Bube first demonstrated the saturation of photocurrent with light intensity in CdS crystals in 1960.[56] The occurrence of the saturation was interpreted as resulting from the saturation of sensitizing energy levels in the crystal. Namely, the centers with a large cross section for holes and a subsequent small cross section for electrons were completely occupied by holes. Additional excited holes generated by further increasing the light intensity could be captured only at centers with large cross section for electrons. Thus the saturated photocurrent was considered to be composed of current arising from long lifetime electrons with density equal to that of sensitizing band and short lifetime electrons produced by absorption of photons over and above those needed to saturate the sensitizing centers. Mueller and co-workers also observed the similar photocurrent saturation in graphene photodetectors.[57] This phenomenon was

Nanoscale Accepted Manuscript

attributed to the screening effect as in conventional photodiodes. In the case of nanowire, the photocurrent saturation at high light intensity can be attributed to the carrier-trap saturation effect.[7] At high light intensity, the density of available carrier-traps exist in the nanowire is cumulatively reduced, resulting in the saturation of the photoresponse. Photoconductivity in semiconducting metal oxide nanowires (such as ZnO) can be attributed to the increased charge carrier by exciting the electrons to the conduction band and the oxygen absorption-desorption process on the nanowire surface.[7, 58, 59] In $W_xV_{1-x}O_2$ nanowires, the photoconductivity can originate from the excitation from the mid gap electronic state introduced by W doping. This mid gap band can be assigned as a donor type photoionization of tungsten dopant which generates delocalized charge carriers upon photoexcitation. Figure 3e shows the reflection spectrum of these nanowires and the spectrum indicates that the nanowires show absorption ranging from UV to IR range. Therefore the $W_xV_{1-x}O_2$ nanowire is anticipated to show photoresponse to multispectral light from UV to NIR. Light from this band can generate mobile charge carriers thereby increasing the charge carrier density, leading to the photocurrent in the nanowires. The other mechanism is oxygen adsorption-desorption where, when the nanowire is excited with photons, the oxygen adsorbed on the nanowire surface is desorbed, releasing the surface bound electrons in the depletion layer and hence increasing the conductance of the nanowire. The oxygen adsorption-desorption effect in this experiment can be considered to be minimal, since we carried out the characterization in high vacuum.

Various photoconductive parameters such as responsivity, external quantum efficiency, photoconductive gain, photocurrent rise time and decay time, and stability of the photocurrent are analyzed to evaluate the performance of a nanowire device as a phototransistor. The phototransistor's responsivity (R_{res}) is defined as the photocurrent per unit power on the effective area of the phototransistor and can be calculated by[60]

$$R_{res} = \frac{I_{pho}}{P_{opt}} = \frac{(I_{illum} - I_{dark})S^{-1}}{P_{inc}} \qquad (1)$$

Where I_{pho} is the photocurrent, P_{opt} is the light power. I_{illum} and I_{dark} are the output current under illumination and in dark, respectively, S is the effective area of nanowire device, and P_{inc} is power density. It is very attractive that the R_{res} value of the $W_xV_{1-x}O_2$ nanowire phototransistor could reach as high as $(2.15 \pm 0.2) \times 10^7$ mAW^{-1} at a light intensity of 50 mW cm^{-2} at 4 V bias. This R_{res} value is much higher than that of grapheme (~ 1 mAW^{-1}),[61] MoS_2 (7.5 mAW^{-1}),[22] and organic (PPEs, 36 mAW^{-1})[17] phototransistors. It is even higher than those of the ZnO nanowires (1.29×10^7 mAW^{-1})[18] and recently reported K_xMoO_3 nanowires (1.75×10^7 mAW^{-1})[62] phototransistors and comparable with vertically aligned Si nanowire arrays (~ 10^8 mAW^{-1})[63]. The high responsivity of the nanowire device enables a large on/off ratio, indicating the potential applications of the nanowire phototransistor in optoelectronic devices such as optoisolators, retrosensors,[16, 64] and photoamplifiers. The related diagram and equivalent circuit of the $W_xV_{1-x}O_2$ nanowire transistor are illustrated in the inset of Figure 3a, where R is the intrinsic resistance of $W_xV_{1-x}O_2$ nanowire.

The photoconductivity enhancement is quantitatively analyzed by calculating the photoconductive gain, which is a critical parameter for evaluating the sensitivity of phototransistors. The photoconductivity gain is defined as the ratio between the number of collected electrons per unit time and the number of absorbed photos per unit time, can be expressed for simplicity as[52]

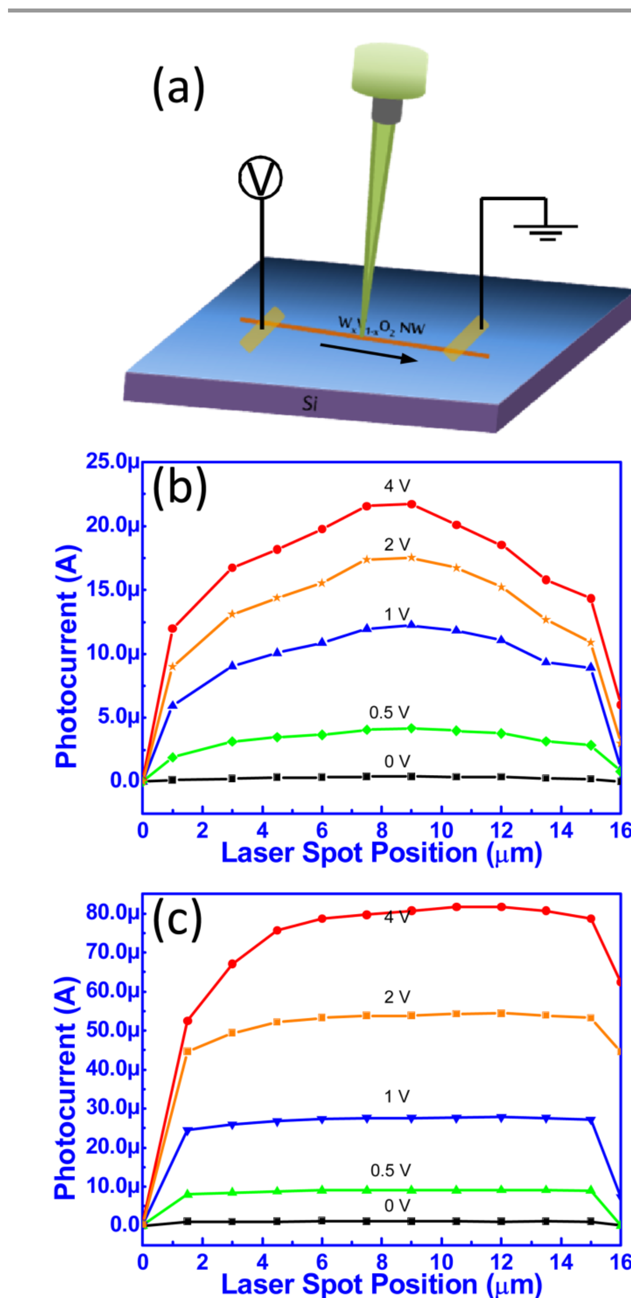

Figure 4. (a) Schematic of the SPCM setup, where the focused laser spot is rastered over the nanowire device. SPCM line scans at different biases under (b) 10 mW cm^{-2} and (c) 30 mW cm^{-2} light intensities. The asymmetrical plot is due to the formation of Schottky contact between the nanowire and the electrode.

Nanoscale Accepted Manuscript

This journal is © The Royal Society of Chemistry 2012

$$G = \frac{N_{ele}}{N_{pho}} = \frac{I_{pho}}{P_{abs}} \times \frac{h\nu}{e} \quad (2)$$

where P_{abs} is the light power absorbed by the effective working area, and $h\nu$ is the energy of an incident photon. Figure 3f shows the calculated photoconductive gain versus various light intensities at 4 V bias. Here, the light power absorbed by the nanowire is lesser than the incident power accordingly. When a laser light incidents onto the interface of two materials with different refractive indices (n_1, n_2), the Fresnel reflection will occur. When the incident light is perpendicular to the interface, the transmission rate can be calculated by $4n_1n_2/(n_1+n_2)^2$.[54] Taking into account the Fresnel reflection from the nanowire, the photoconductive gain can be calculated and the gain decreases with increasing light intensity. Similar as the increasing photocurrent with light intensity, at lower light intensity (<100 mW cm^{-2}), the relationship between the photoconductive gain and the light intensity can be described with an inverse power law with a fractional power dependence of the gain in $W_xV_{1-x}O_2$ nanowires ($G \sim P^{-1.5}$). At higher light intensity, the photoconductive gain deviates below this power law dependence. The decreasing photoconductive gain results mainly from the carrier trap saturation effect. Under such saturation condition, the photoconductive gain can also be derived and expressed for simplicity as[7]

$$G = \frac{I_{pho}}{eF} = (\frac{T_1}{T_t})\frac{1}{1+(F/F_0)^n} \quad (3)$$

where F is the photon absorption rate, F_0 is the absorption rate when trap saturation occurs, T_1 is the carrier life time, and T_t is the carrier transit time. The first term on the right-hand side is the usual description for the photoconductive gain, which is the ratio of carrier life time to carrier transit time, whilst the second term describes trap saturation at high excitation intensities. As displayed in Figure 3f, the extremely long photocarrier life time accompanied by the short carrier transit time due to the small dimensionality of the nanowire device facilitates photoconductive gain as high as G = 1.8 × 10^5. The decrease of the gain at relatively high light intensities is a manifestation of trap saturation. In addition to this reason, the onset of carrier recombination at the high light intensity may also contribute to the shortening of the carrier life time.[7, 65] To determine the carrier life time, the SPCM setup was employed to carry out the line scans rastered over the nanowire device. Figure 4a schematically illustrates the SPCM setup where a focused micro-size laser spot is scanned along the $W_xV_{1-x}O_2$ nanowire. The photocurrent profiles under different applied bias ranging from 0 V to 4 V with lower light intensity (10 mW cm^{-2}) and higher light intensity (30 mW cm^{-2}) irradiation are shown in Figure 4b and c, respectively. Evidently, the most apparent difference of the photocurrent profile under bias with different light intensity is the appearance of higher magnitude around the center of the nanowire in Figure 4b, whilst the profile is almost flat in Figure 4c. This observed photocurrent profile under applied bias is an indication that the carrier life time at low light

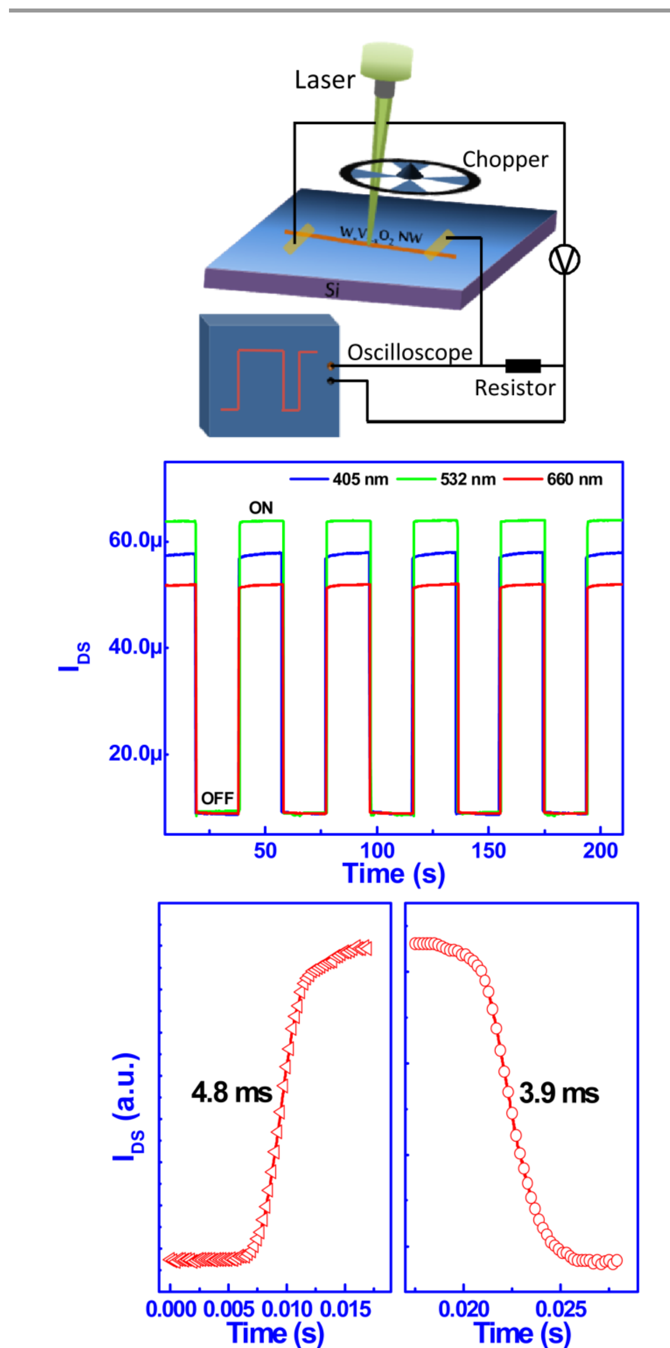

Figure 5. (a) Schematic diagram of time response measurement setup. (b) Photoresponse characteristics at different wavelength. (c) and (d) Photoswitching rate test of the device.

intensity is significantly longer than that at higher light intensity in $W_xV_{1-x}O_2$ nanowires. Yu and co-workers [66] attributed this feature of the photocurrent profiles to long carrier life times in VO_2 nanobelts with similar SPCM results, supported with the experimental results and a numerical simulation of the electrodynamics of free carriers in 1D nanostructures under steady state local illumination, following the method described in Ref. [67]. For a given 1D system, local irradiation usually generates nonequilibrium carriers with lower densities. If the carriers possessed short life time, the

Nanoscale Accepted Manuscript

photocurrent profile had a flat line shape with no discernible peak, as shown in Figure 4c. This is because that the nonequilibrium carriers with short life time would not reach the electrodes. However, when the carrier life time is long enough, even weak illumination could generate a high nonequilibrium carrier densities, since the recombination rate is low enough to allow a high density of carriers to accumulate in the steady state.[66] In this case, the photocurrent profile under bias develops a broad peak and the peak is located where the real current switches from being dominated by the electron current to being dominated by the hole current.[37]

The promising phototransistor performance is also supported by the ultrafast photoresponse of $W_xV_{1-x}O_2$ nanowire to light illumination, which determines the capability of the device to follow fast-varying optical signals. The rapid response time was detected by an oscilloscope (DSO-X 3024A, 200 MHz) associated with an electronic chopper (SRS SR540). The experimental setup is schematically illustrated in Figure 5a. In this setup, the light chopper was employed to turn the laser on and off while the oscilloscope was utilized to monitor the time dependence of the output current. The transient response of the transistor has been investigated under applied bias of 1 V with different wavelength light of 405 nm, 532 nm, and 660 nm, respectively. Illumination was switched on and off periodically. As shown in Figure 5b, the device shows a rapid on/off switching behavior. Each photoresponse cycle consists of three distinct stages, a sharp rise, a steady state, and a sharp decay process to original state with the amplification ratios, $(I_{pho} - I_{dark})/I_{dark}$, ranging from 1667% to 2300% under 87.5 mW cm^{-2} illumination. The fast photocurrent rise and decay time was estimated from the photocurrent versus time plots and shown in Figure 5c and d, respectively. The rise time is defined as the time needed to reach 90% of the photocurrent from dark current upon laser irradiation, and the decay time is defined as the time needed to decay the current value to 10% after switching of the light. Accordingly, 4.8 ms of the rise and 3.9 ms of the decay times were measured. These rapid frequencies (0.21 and 0.26 kHz) are much faster than that of the reported organic (F16CuPc, 50 Hz andand TA-PPE, 100 Hz) and inorganic (ZnO) phototransistors and photoswithces.[16-18] It is even slightly faster than the recently reported K_xMoO_3 and TiO_2/C core/shell nanowires.[62, 68]. The 3 dB bandwidth (f_{3dB}) of the present device can be calculated to be about 0.73 kHz from the expression of $f_{3dB} = 0.35/t_r$.[52] This fast response frequency and wide response range indicate the great potential of $W_xV_{1-x}O_2$ nanowires as the building-block in the ultrafast nano-optoelectronic devices.

Conclusions

In conclusion, a simple, low cost but effective hydrothermal approach was developed and employed to synthesize high quality single crystalline $W_xV_{1-x}O_2$ nanowires with high yield. Based on these nanowires, single nanowire phototransistors were fabricated and systematically characterized. The extreme shallow donor created by the doping of W enables an ultrasensitive and superfast photocurrent response. The characteristic curves of the device demonstrated that the saturation of the output current can be achieved within a voltage window of 1.5 V, and light is able to serve as a control over the current level, facilitating the applications of this single nanowire device as a promising phototransistor and photosensor. Moreover, the high responsivity and broad multispectral response further show the potential of this material in the nano-optoelectronic applications for sensing, imaging and communications.

Acknowledgements

This work is supported by the Singapore National Research Foundation under CRP Award No. NRF-CRP-4-2008-03. The authors also acknowledge the support from the NUS FRC Grant No. R-144-000-281-112.

Notes and references

[a] Department of Physics, 2 Science Drive 3, National University of Singapore, 117542, Singapore. Email: physowch@nus.edu.sg
[b] Institute of Materials Research and Engineering, A*STAR (Agency for Science, Technology and Research), 3 Research Link, 117602, Singapore.
[c] Department of Electrical and Electronic Engineering, South University of Science and Technology of China, 1088 Xueyuan Road, Xili, Nanshan District, Shenzhen, Guangdong, China 518055. Email: zhang.xh@sustc.edu.cn
[d] School of Materials Science and Engineering, Nanyang Technological University, Blk N4.1, Nanyang Avenue, 639798, Singapore.
† These authors make equal contribution to this work.

1. L. Peng, L. Hu and X. Fang, *Adv. Mater.*, 2013, **25**, 5321.
2. S.-B. Wang, R.-S. Chen, S. J. Chang, H.-C. Han, M.-S. Hu, K.-H. Chen and L.-C. Chen, *Nanoscale*, 2014, **6**, 1264.
3. X. Fang, Y. Bando, M. Liao, U. K. Gautam, C. Zhi, B. Dierre, B. Liu, T. Zhai, T. Sekiguchi, Y. Koide and D. Golberg, *Adv. Mater.*, 2009, **21**, 2034.
4. L. Hu, M. M. Brewster, X. Xu, C. Tang, S. Gradečak and X. Fang, *Nano Lett.*, 2013, **13**, 1941.
5. X. Fang, S. Xiong, T. Zhai, Y. Bando, M. Liao, U. K. Gautam, Y. Koide, X. Zhang, Y. Qian and D. Golberg, *Adv. Mater.*, 2009, **21**, 5016.
6. W. Wang, J. Qi, Q. Wang, Y. Huang, Q. Liao and Y. Zhang, *Nanoscale*, 2013, **5**, 5981.
7. C. Soci, A. Zhang, B. Xiang, S. A. Dayeh, D. P. R. Aplin, J. Park, X. Y. Bao, Y. H. Lo and D. Wang, *Nano Lett.*, 2007, **7**, 1003.
8. J. S. Jie, W. J. Zhang, Y. Jiang, X. M. Meng, Y. Q. Li and S. T. Lee, *Nano Lett.*, 2006, **6**, 1887.
9. C. Soci, A. Zhang, X.-Y. Bao, H. Kim, Y. Lo and D. Wang, *J. Nano Sci. Nanotechno.*, 2010, **10**, 1430.
10. H. Kind, H. Yan, B. Messer, M. Law and P. Yang, *Adv. Mater.*, 2002, **14**, 158.
11. L. Hu and G. Chen, *Nano Lett.*, 2007, **7**, 3249.
12. W. U. Huynh, J. J. Dittmer and A. P. Alivisatos, *Science*, 2002, **295**, 2425.

Nanoscale Accepted Manuscript

This journal is © The Royal Society of Chemistry 2012

13. B. Tian, T. J. Kempa and C. M. Lieber, *Chem. Soc. Rev.*, 2009, **38**, 16.
14. A. J. Seeds and A. A. A. de Salles, *IEEE T. Microw. Theory*, 1990, **38**, 577.
15. T. P. I. Saragi, R. Pudzich, T. Fuhrmann and J. Salbeck, *Appl. Phys. Lett.*, 2004, **84**, 2334.
16. Q. Tang, L. Li, Y. Song, Y. Liu, H. Li, W. Xu, Y. Liu, W. Hu and D. Zhu, *Adv. Mater.*, 2007, **19**, 2624.
17. H. Dong, H. Li, E. Wang, H. Nakashima, K. Torimitsu and W. Hu, *J. Phys. Chem. C*, 2008, **112**, 19690.
18. W. Y. Weng, S. J. Chang, C. L. Hsu and T. J. Hsueh, *ACS Appl. Mater. Interfaces*, 2011, **3**, 162.
19. T. B. Singh, R. Koeppe, N. S. Sariciftci, M. Morana and C. J. Brabec, *Adv. Funct. Mater.*, 2009, **19**, 789.
20. A. Zhang, S. You, C. Soci, Y. Liu, D. Wang and Y.-H. Lo, *Appl. Phys. Lett.*, 2008, **93**, 121110.
21. Y. Guo, C. Du, C.-a. Di, J. Zheng, X. Sun, Y. Wen, L. Zhang, W. Wu, G. Yu and Y. Liu, *Appl. Phys. Lett.*, 2009, **94**, 143303.
22. Z. Yin, H. Li, H. Li, L. Jiang, Y. Shi, Y. Sun, G. Lu, Q. Zhang, X. Chen and H. Zhang, *ACS Nano*, 2011, **6**, 74.
23. B. S. Guiton, Q. Gu, A. L. Prieto, M. S. Gudiksen and H. Park, *J. Am. Chem. Soc.*, 2004, **127**, 498.
24. J. I. Sohn, H. J. Joo, A. E. Porter, C.-J. Choi, K. Kim, D. J. Kang and M. E. Welland, *Nano Lett.*, 2007, **7**, 1570.
25. J. M. Baik, M. H. Kim, C. Larson, A. M. Wodtke and M. Moskovits, *J. Phys. Chem. C*, 2008, **112**, 13328.
26. L. Whittaker, C. Jaye, Z. Fu, D. A. Fischer and S. Banerjee, *J. Am. Chem. Soc.*, 2009, **131**, 8884.
27. J. Liu, Q. Li, T. Wang, D. Yu and Y. Li, *Angew. Chem. Int. Ed.*, 2004, **43**, 5048.
28. M. Netsianda, P. E. Ngoepe, C. R. A. Catlow and S. M. Woodley, *Chem. Mater.*, 2008, **20**, 1764.
29. K. Shibuya, M. Kawasaki and Y. Tokura, *Appl. Phys. Lett.*, 2010, **96**, 022102.
30. I. P. Parkin and T. D. Manning, *J. Chem. Educ.*, 2006, **83**, 393.
31. C. Tang, P. Georgopoulos, M. E. Fine, J. B. Cohen, M. Nygren, G. S. Knapp and A. Aldred, *Phys. Rev. B*, 1985, **31**, 1000.
32. L. Whittaker, T.-L. Wu, C. J. Patridge, G. Sambandamurthy and S. Banerjee, *J. Mater. Chem.*, 2011, **21**, 5580.
33. L. Whittaker, T.-L. Wu, A. Stabile, G. Sambandamurthy and S. Banerjee, *ACS Nano*, 2011, **5**, 8861.
34. M. C. Putnam, D. B. Turner-Evans, M. D. Kelzenberg, S. W. Boettcher, N. S. Lewis and H. A. Atwater, *Appl. Phys. Lett.*, 2009, **95**, 163116.
35. Y. Ahn, J. Dunning and J. Park, *Nano Lett.*, 2005, **5**, 1367.
36. R. Graham, C. Miller, E. Oh and D. Yu, *Nano Lett.*, 2010, **11**, 717.
37. Y. Gu, J. P. Romankiewicz, J. K. David, J. L. Lensch and L. J. Lauhon, *Nano Lett.*, 2006, **6**, 948.
38. J. E. Allen, E. R. Hemesath and L. J. Lauhon, *Nano Lett.*, 2009, **9**, 1903.
39. Y. H. Ahn, A. W. Tsen, B. Kim, Y. W. Park and J. Park, *Nano Lett.*, 2007, **7**, 3320.
40. Y.-J. Doh, K. N. Maher, L. Ouyang, C. L. Yu, H. Park and J. Park, *Nano Lett.*, 2008, **8**, 4552.
41. J. M. Atkin, S. Berweger, E. K. Chavez, M. B. Raschke, J. Cao, W. Fan and J. Wu, *Phys. Rev. B*, 2012, **85**, 020101.
42. D. B. McWhan, M. Marezio, J. P. Remeika and P. D. Dernier, *Phys. Rev. B*, 1974, **10**, 490.
43. H. Kuzmany, *Solid State Spectroscopy*, Springer, New York, 1998.
44. C. Marini, E. Arcangeletti, D. Di Castro, L. Baldassare, A. Perucchi, S. Lupi, L. Malavasi, L. Boeri, E. Pomjakushina, K. Conder and P. Postorino, *Phys. Rev. B*, 2008, **77**, 235111.
45. J. Cao, Y. Gu, W. Fan, L. Q. Chen, D. F. Ogletree, K. Chen, N. Tamura, M. Kunz, C. Barrett, J. Seidel and J. Wu, *Nano Lett.*, 2010, **10**, 2667.
46. P. Schilbe, *Physica B*, 2002, **316–317**, 600.
47. J. Y. Chou, J. L. Lensch-Falk, E. R. Hemesath and L. J. Lauhon, *J. Appl. Phys.*, 2009, **105**, 034310.
48. H. W. Liu, L. M. Wong, S. J. Wang, S. H. Tang and X. H. Zhang, *J. Phys.: Condens. Matter*, 2012, **24**, 415604.
49. M. Imada, A. Fujimori and Y. Tokura, *Rev. Mod. Phys.*, 1998, **70**, 1039.
50. K. Joondong, Y. Ju-Hyung, K. Chang Hyun, P. Yun Chang, W. Ju Yeon, P. Jeunghee, L. Jung-Ho, Y. Junsin and H. Chang-Soo, *Nanotechnology*, 2010, **21**, 115205.
51. A. Tselev, E. Strelcov, I. A. Luk'yanchuk, J. D. Budai, J. Z. Tischler, I. N. Ivanov, K. Jones, R. Proksch, S. V. Kalinin and A. Kolmakov, *Nano Lett.*, 2010, **10**, 2003.
52. S.-C. Kung, W. E. van der Veer, F. Yang, K. C. Donavan and R. M. Penner, *Nano Lett.*, 2010, **10**, 1481.
53. J.-J. Wang, F.-F. Cao, L. Jiang, Y.-G. Guo, W.-P. Hu and L.-J. Wan, *J. Am. Chem. Soc.*, 2009, **131**, 15602.
54. P. Wu, Y. Dai, Y. Ye, Y. Yin and L. Dai, *J. Mater. Chem.*, 2011, **21**, 2563.
55. K. S. Stevens, M. Kinniburgh and R. Beresford, *Appl. Phys. Lett.*, 1995, **66**, 3518.
56. R. H. Bube, *J. Appl. Phys.*, 1960, **31**, 1301.
57. T. Mueller, F. Xia and P. Avouris, *Nat. Photon.*, 2010, **4**, 297.
58. N. Mathews, B. Varghese, C. Sun, V. Thavasi, B. P. Andreasson, C. H. Sow, S. Ramakrishna and S. G. Mhaisalkar, *Nanoscale*, 2010, **2**, 1984.
59. S. Mathur, S. Barth, H. Shen, J.-C. Pyun and U. Werner, *Small*, 2005, **1**, 713.
60. X. Fang, L. Hu, K. Huo, B. Gao, L. Zhao, M. Liao, P. K. Chu, Y. Bando and D. Golberg, *Adv. Funct. Mater.*, 2011, **21**, 3907.
61. F. Xia, T. Mueller, Y.-m. Lin, A. Valdes-Garcia and P. Avouris, *Nat Nano*, 2009, **4**, 839.
62. J. Lu, C. Sun, M. Zheng, Y. Wang, M. Nripan, J. A. van Kan, S. G. Mhaisalkar and C. H. Sow, *J. Phys. Chem. C*, 2012, **116**, 22015.
63. A. Zhang, H. Kim, J. Cheng and Y.-H. Lo, *Nano Lett.*, 2010, **10**, 2117.
64. M. C. Hamilton, S. Martin and J. Kanicki, *IEEE T. Electron Dev.*, 2004, **51**, 877.
65. C. Soci, D. Moses, Q.-H. Xu and A. J. Heeger, *Phys. Rev. B*, 2005, **72**, 245204.
66. C. Miller, M. Triplett, J. Lammatao, J. Suh, D. Fu, J. Wu and D. Yu, *Phys. Rev. B*, 2012, **85**, 085111.
67. M. Rini, Z. Hao, R. W. Schoenlein, C. Giannetti, F. Parmigiani, S. Fourmaux, J. C. Kieffer, A. Fujimori, M. Onoda, S. Wall and A. Cavalleri, *Appl. Phys. Lett.*, 2008, **92**, 181904.
68. C.-Y. Hsu, D.-H. Lien, S.-Y. Lu, C.-Y. Chen, C.-F. Kang, Y.-L. Chueh, W.-K. Hsu and J.-H. He, *ACS Nano*, 2012, **6**, 6687.

Nanoscale Accepted Manuscript